Supplementary materials to:

In Situ Remodeling Overrules Bioinspired Scaffold Architecture of Supramolecular Elastomeric Tissue-Engineered Heart Valves.

Authors: M. Uiterwijk, MD[¶], A.I.P.M. Smits, PhD[¶] , D. van Geemen, PhD, B. van Klarenbosch, MD, S. Dekker, MSc, M.J. Cramer, MD PhD, J.W. van Rijswijk, MSc, E.B. Lurier, PhD, A. Di Luca, PhD, M.C.P. Brugmans, PhD, T. Mes, PhD, A.W. Bosman, PhD, E. Aikawa, MD PhD, P.F. Gründeman, MD PhD, C.V.C Bouten, PhD[¶,c], J.Kluin, MD PhD[¶,c]

[¶]Authors contributed equally

[c]Corresponding authors:

Prof. C.V.C. (Carlijn) Bouten; c.v.c.bouten@tue.nl

Prof. J. (Jolanda) Kluin; j.kluin@amsterdamumc.nl

DETAILED METHODS

Production and Characterization of Electrospun Valvular Scaffolds

Valve manufacturing

The valvular scaffolds were fabricated from ureidopyrimidinone-polycarbonate (UPy-PC). UPy-PC is a bioresorbable supramolecular polymer, which is formed by arrays of directed, noncovalent interactions between the building blocks[1]. The blocks comprise a poly(hexamethylene carbonate) diol chain extended with 2-ureido-[1H]-pyrimidin-4-one motifs[2]. The UPy-PC was processed into a highly porous tubular conduit via electrospinning in a climate controlled electrospinning chamber (IME Technologies). Scaffolds were spun with either a random fiber alignment or with fibers aligned in the circumferential direction (referred to as rTEHV and aTEHV, respectively).

Subsequently, the electrospun tubular conduits were sutured onto a crown-shaped polyether ether ketone (PEEK) supporting ring (inner diameter 18 mm, outer diameter 20 mm) to create a tri-leaflet valvular shape, as previously described in detail[3]. Scaffold thickness was measured with a digital thickness gauge (Mitutoyo SGM). The scaffold microarchitecture was evaluated in terms of average fiber diameter and the extent of fiber alignment via scanning electron microscopy (SEM; Phenom World Phenom Pro, FibermetricR software). The extent of fiber alignment was quantified from the SEM images as previously described in detail[4]. In brief, The SEM images were binarized and the principal direction in each pixel were calculated and binned into a histogram ranging from 0 to 180 degrees, with 0 degrees representing the axial direction of the cylindrical electrospun tube and 90 degrees representing the circumferential direction of the tubular scaffold. These angles correspond to the radial and circumferential direction of the valve leaflet, respectively, after fabricating the valve from the tube. The histograms were parameterized by fitting a normalized Gaussian distribution with an additional baseline. This generated three parameters, namely (1) the main fiber angle, (2) the fraction of randomly oriented fibers under the baseline, and (3) the fraction of aligned fibers under the peak in the principle direction. These parameters were determined for both groups (at least N = 8 scaffolds

per group) and averaged per group. After fabrication, the valves were sterilized by gamma irradiation (25 kGray; Synergy health).

Hydrodynamic in vitro functionality assessment of fabricated valves

To assess *in vitro* valve functionality, one rTEHV and one aTEHV were placed inside a silicone annulus of 20 or 21 mm inner diameter and positioned into a hydrodynamic pulsatile duplicator system (HDT-500, BDC laboratories) containing physiological saline solution at 37 °C. The valve was subjected to physiological pulmonary conditions (rate of 72 bpm, stroke volume of 70 ml, max diastolic pressure difference of 25 mmHg) for 1 hour. Flow and pressure were monitored via an ultrasonic flow probe (TS410, Transonic Systems) and pressure sensors (BDC-TP, BDC Laboratories), respectively. Data was collected for 5 s at 5 kH and functionality was assessed from an average over 10 cardiac cycles by using Statys software (BDC Laboratories) to determine cardiac output (CO) and effective orifices area (A_{EO}), as well as stroke, leakage and closing volume. Slow motion movies were recorded to assess opening and closing behaviour of the valve as well as leaflet motion.

Pulmonary Valve Implantation in the Ovine Model

Animals and surgical procedure

The animal experiments were approved by the Animal Care Ethics committee of the University Medical Center Utrecht and were performed in agreement with the current Dutch law on animal experiments. Twenty female swifter sheep (mean weight 52.0 ± 4.6 kg, mean age 13.6 ± 1.0 months, mean pulmonary valve annulus size 24.7 ± 1.3 mm) underwent pulmonary valve replacement. The scheduled follow-up period was 1 month (n=2), 6 months (n=4) and 12 months (n=4) in each group (rTEHV and aTEHV; 20 animals in total). The surgical procedures were performed in an experienced animal laboratory with a team of surgeons (J.K., P.G.) and fellow workers. Buprenorphine (5 mcg/hr patch; BuTrans, mundipharma DC) and Diazepam (10 mg orally, Diazepam CF, Centrafarm) was given as premedication on the day of surgery.

Ketamine/hydrochlorin (10 mg/kg IM; Narketan 10, Vetoquinol) and Midazolam (0.75 mg/kg IM; Midazolam Actavis 5 mg/ml, Actavis) was given intramusculary prior to surgery. Propofol was used as induction anesthesia (2-4 mg/kg; Propofol 20 mg/ml, Fresenius Kabi). Propofol (4-7 mg/kg; Propofol 20 mg/ml, Fresenius Kabi) and Sufenta forte (5 µg/kg Sufentanil – Hamelnm 50 mcg/ml, Hameln) was given to maintain anesthesia during surgery. Furthermore, prophylactic Amiodarone (150 mg; Cordarone 50 mg/ml, Sanofi-aventis) was given intravenously to prevent arrhythmias. During surgery, animals were monitored in terms of electrocardiography (ECG), arterial blood pressure, capnography, and temperature. For the implantation procedure, animals were placed in the right lateral position. Heparin was administered intravenously. After induction of anesthesia the animals were placed on cardiopulmonary bypass. For arterial access, a 16 FR arterial cannula (Edwards Lifesciences) was placed in the left carotid artery. A 24 FR venous cannula was placed in the left jugular vein. Subsequently, a left thoracotomy was performed. After dissection of the pericardium a longitudinal incision in the pulmonary artery was made distally from the native pulmonary valve. The native valve leaflets were excised. The biodegradable electrospun heart valve prosthesis was implanted using continuous suture (5-0). After careful de-airing, the pulmonary artery was closed in a continuous fashion. Protamine was administered intravenously and the cannulas were removed. A chest tube was placed in the left thoracic cavity and the wound was closed in two layers. Furosemide (2 dd 20 mg; Furosemide 20 PHC, pharmachemie BV) and Flunixinenemglumine (1 dd 0.02 ml/kg; Cronyxin, 50 mg/ml, Dechra) was given during the first three days post-operatively. Animals received Ascal (1 dd 80 mg orally; Ratiopharm) for 3 months. At the end of follow-up the animals were exsanguinated under full anaesthesia, after which the implanted TEHV were explanted.

Functional valve evaluation

Functional valve evaluation was asses invasively and non-invasively manners.

Baseline cardiac and valve function of all animals was conducted non-invasively with transthoracic echocardiography (TTE), before the implantation procedure in the operating room

while animals were on full anaesthesia. During the procedure, before closing, blood pressures were measured invasively distal and proximal to the implanted valve (Digital ultrasonic measurement system, Argon BV, Spacelab) during 3 cardiac cycles for transvalvular pressure gradient analyses. Next a epicardial echocardiogram was performed to conduct baseline measurement of the implanted valve. During follow-up, valve functionality was evaluated in all animals by TTE at 2, 4, 6 and 9 months in their dome, while the animals were fully awake. At time of explantation, functional evaluation was repeated in similar fashion as at time of implantation. Echo recordings were qualitatively evaluated on leaflet motion, signs of endocarditis and severity of pulmonary regurgitation (grade 1-3), mainly based on regurgitant jet area, by two clinicians (B.v.K., M.J.C.) in blinded fashion. In addition, quantitative assessment was performed by manually tracing continuous wave (CW) Doppler derived flow velocity curves, by which the peak- and mean transvalvular flow velocities were measured. Using the simplified Bernoulli equation ($\Delta p = 4V^2$) transvalvular peak- and mean pressure gradients were derived. In addition, pulsed wave (PW) derived flow velocity in the right ventricular outflow tract was measured, allowing for the estimation of the pulmonary valve area (PVA) using the continuity equation

Explant Evaluation

After explantation, valves were macroscopically evaluated for signs of valve thrombosis, structural valve deterioration (refers to changes intrinsic to the valve such as leaflet tear, wear or retraction) and non-structural deterioration (such as entrapment by pannus tissue or cusp/wall fusion), according to the guidelines reporting morbidity and mortality after cardiac valve interventions[5]. Thereafter a suture for orientation was placed between the anterior and the left leaflet, and the valve was carefully resected from the PEEK-reinforcement ring. The valve was cut in longitudinal direction between the commissures of the left and right cusp to expose the leaflets, and photos were taken for gross morphology assessment. The valve was then transected for further analysis according to a predefined cutting scheme (Fig. S1).

Histology

Formalin-fixed, paraffin-embedded valve specimens were sectioned at 4 µm. Next, the sections were stained with Weigert's Hematoxylin and Eosin (H&E) for visualizing overall morphology, Masson's Trichrome for extracellular matrix, picrosirius red for collagen, Elastin van Gieson for mature elastic fibers, and von Kossa for mineral deposition. All histological stainings were performed according to the local standard operating procedures (SOP). All stained sections were digitized using a Philips Ultra Fast Scanner (Philips Digital Pathology Solutions, Best, the Netherlands) and high-resolution images were saved as Tiff (resolution: 4 pixels/µm). Cellularity was studied in the hinge, belly and tip portions of the leaflet at 40x magnification and analyzed using ImageJ software[6]. To quantify the amount of collagen, regions of interest (ROI) were drawn, specifying the pulmonary, scaffold and ventricular layers, segmented and analyzed using ImageJ software. The average collagen value per ROI was expressed as percentage of total surface area (area fraction). Moreover, cross sections of leaflet samples stained with picrosirius red were imaged with polarized light microscopy to visualize the collagen fiber alignment trough all layers of the leaflet. Mineral deposition was quantified as microscopic (< 0.5 mm^2) or macroscopic (> 0.5 mm^2) in size. Elastin was scored as none (grade 0), a few thin fibers (grade 1), moderate thin (grade 2), or native like dense fibers (grade 3) (Fig. S2). Histological analyses were conducted by two reviewers in blinded fashion (J.W.R. & M.U.).

En face collagen alignment in superficial layers

To visualize the alignment of collagen at the superficial layers (*en face*) of the pulmonary and ventricular leaflet side, part of the leaflet was stained overnight with the fluorescent collagen probe CNA35-mCherry[7,8]. The collagen alignment on both sides of the valve was visualized using a confocal laser scanning microscope (TCS SP5X, Leica Microsystems). An array of z-stacks was taken from the surface of the valve (pulmonary and ventricular side) into the tissue. To quantify the collagen fiber orientation, the individual images of each z-stack were analysed

according to the same methods as the alignment of the scaffold anisotropy. The number and direction of the collagen fiber were converted into a fiber fraction per angle, resulting in an orientation histogram per side of the leaflet for each valve. To capture the collagen architecture of the excised part of the leaflet in one single image, the maximum projections of the z-stacks were composed into a tile scan (10x magnification).

Surface coverage and endothelialisation

To assess neo-tissue coverage and endothelialisation of the implanted scaffolds, samples were fixed in glutaraldehyde (2.5%) and dehydrated in a graded ethanol series, starting from 50% to 100% in 5–20% increments. The ethanol was then allowed to evaporate, and samples were gold-sputtered for visualization by SEM (Quanta 600F, FEI).

Biaxial tensile tests

The mechanical properties of the non-implanted control scaffolds (with random or aligned fibers) and the explants were determined by using a biaxial tensile tester (BioTester, 1.5 N load cell; CellScale) in combination with LabJoy software (V8.01, CellScale). To test the properties of the control scaffolds, squared test samples (10 x 10 mm^2) were cut from left-over pieces of the electrospun tube (after manufacturing the valve). One square sample (10 x 10 mm^2) per explanted valve was symmetrically cut from the belly region to analyse the mechanical properties of the valve leaflet. The averaged sample thickness was assessed by measuring the thickness using an electronic calliper (CD-15CPX, Mitutoyo) at 3 random locations. The samples were stretched equibiaxially in the radial and circumferential direction up to an step-wise increasing maximum strain at a strain rate of 100% per minute, followed by recovery to 0% strain at a strain rate of 100% per minute and a rest cycle of 54 seconds. For each maximum strain level, 5 cycles were performed. For each sample, the (engineering) stresses and strains in radial and circumferential direction were determined from the last cycle, up to 25% strain. The average stress-strain curves were plotted per group (aTEHV and rTEHV), per time point. From

the stress-strain curves, the tangent moduli were determined in the low-strain (5%) and high-strain (15%) regimes. The anisotropy ratios at these strains were calculated as the ratio of the tangent modulus in the circumferential direction over the tangent modulus in radial direction.

In situ *resorption of scaffold fibers*

To evaluate scaffold resorption, explanted samples were treated with 4.6 % sodium hypochlorite (Clorox) for 10 minutes at room temperature and washed twice in purified water, to remove all cells and newly formed tissue, without affecting the scaffold fiber morphology. Clorox-treated samples were analysed with SEM for visual assessment of fiber resorption and with Gel Permeation Chromotography (GPC) to measure the molecular weight of the remaining polymer. For SEM visualisation, samples were dehydrated and mounted on aluminium stubs. The average fiber diameter was determined by SEM (Phenom World Phenom Pro, FibermetricR software) images for each explant by measuring at least 10 fibers at a magnification of 3500x. For GPC, poly(ethylene) glycol standards (PSS, Mainz Germany) were analysed to generate the calibration curve. 10-20 mg of the scaffold material was dissolved at 50 °C in a dimethylformamide/lithiumbromide solvent mixture. 50 µL of each solution was injected into the column (temperature set at 70 °C) at a flow rate of 1.0 mL/min. A 10 µm guard unit, a mixed column (30 – 3000 Å) and differential refractometer detector was used the GPC setup. PSS Win GC unichrom software was used to collect and analyse the data. The weight-averaged molecular weight (M_w) and number-averaged molecular weight (M_n) were determined, from which the dispersity (D) was calculated (M_w/M_n).

Biochemical analysis of matrix components and DNA content

Tissue samples were incubated overnight at 60 °C in a papain digestion buffer (Sigma). Thereafter, the amount of DNA was quantified using the Hoechst dye method[9], with a reference curve prepared from calf thymus DNA (Sigma). A modification of the assay described by

Farndale et al., with shark cartilage chondroitin sulfate as a reference, was used to measure the glycosaminoglycan (GAG) content[10]. To determine the hydroxyproline (HYP) quantity, as a measure for collagen content, the assay according to Huszar et al. with trans-4-hydroxyproline (Sigma) was used[11]. The (tropo)elastin content was assessed using the Fastin Elastin assay (Biocolor) according to the manufacturer's protocol. To this end, five digestions were performed for each sample in order to ensure quantification of the complete (tropo)elastin content.

References

1. Sijbesma RP, Beijer FH, Brunsveld L, Folmer BJ, Hirschberg JH, Lange RF, Lowe JK, Meijer EW. Reversible polymers formed from self-complementary monomers using quadruple hydrogen bonding. *Science*. 1997;278:1601–4.
2. Söntjens SHM, Renken RAE, van Gemert GML, Engels TAP, Bosman AW, Janssen HM, Govaert LE, Baaijens FPT. Thermoplastic Elastomers Based on Strong and Well-Defined Hydrogen-Bonding Interactions. *Macromolecules*. 2008;41:5703–5708.
3. Kluin J, Talacua H, Smits AIPM, Emmert MY, Brugmans MCP, Fioretta ES, Dijkman PE, Söntjens SHM, Duijvelshoff R, Dekker S, Janssen-van den Broek MWJT, Lintas V, Vink A, Hoerstrup SP, Janssen HM, Dankers PYW, Baaijens FPT, Bouten CVC. In situ heart valve tissue engineering using a bioresorbable elastomeric implant – From material design to 12 months follow-up in sheep. *Biomaterials*. 2017;125:101–117.
4. Van Haaften EE, Wissing TB, Rutten MCM, Bulsink JA, Gashi K, van Kelle MAJ, Smits AIPM, Bouten CVC, Kurniawan NA. Decoupling the Effect of Shear Stress and Stretch on Tissue Growth and Remodeling in a Vascular Graft. *Tissue Eng Part C Methods*. 2018;24:418–429.
5. Akins CW, Miller DC, Turina MI, Kouchoukos NT, Blackstone EH, Grunkemeier GL, Takkenberg JJM, David TE, Butchart EG, Adams DH, Shahian DM, Hagl S, Mayer JE, Lytle BW, STS, AATS, EACTS. Guidelines for reporting mortality and morbidity after cardiac valve interventions. *Ann Thorac Surg*. 2008;85:1490–5.
6. Schindelin J, Arganda-Carreras I, Frise E, Kaynig V, Longair M, Pietzsch T, Preibisch S, Rueden C, Saalfeld S, Schmid B, Tinevez J-Y, White DJ, Hartenstein V, Eliceiri K, Tomancak P, Cardona A. Fiji: an open-source platform for biological-image analysis. *Nat Methods*. 2012;9:676–82.
7. Krahn KN, Bouten CVC, Van Tuijl S, Van Zandvoort MAMJ, Merkx M. Fluorescently labeled collagen binding proteins allow specific visualization of collagen in tissues and live cell culture. *Anal Biochem*. 2006;350:177–185.
8. Aper SJA, van Spreeuwel ACC, van Turnhout MC, van der Linden AJ, Pieters PA, van der Zon NLL, de la Rambelje SL, Bouten CVC, Merkx M. Colorful protein-based fluorescent probes for collagen imaging. *PLoS One*. 2014;9:e114983.
9. Cesarone CF, Bolognesi C, Santi L. Improved microfluorometric DNA determination in biological material using 33258 Hoechst. *Anal Biochem*. 1979;100:188–97.
10. Farndale RW, Buttle DJ, Barrett AJ. Improved quantitation and discrimination of sulphated glycosaminoglycans by use of dimethylmethylene blue. *Biochim Biophys Acta*. 1986;883:173–7.
11. Huszar G, Maiocco J, Naftolin F. Monitoring of collagen and collagen fragments in chromatography of protein mixtures. *Anal Biochem*. 1980;105:424–9.

SUPPLEMENTARY TABLES

Table S1. *In vitro* functionality test of random (rTEHV) and aligned (aTEHV) heart valve scaffolds using a 20 mm ∅ holder. Data represent the mean ± standard deviation of 10 consecutive cycles.

	rTEHV	**aTEHV**
General configuration		
Stroke Volume [mL]	62.77 ± 0.07	62.90 ± 0.07
Cardiac Output [L/min]	5.00 ± 0.03	5.26 ± 0.01
Open configuration		
Calculated A_{EO} [cm^2]	1.43 ± 0.01	1.26 ± 0.01
Closed configuration		
Regurgitation fraction [%]	10.1 ± 0.8	15.7 ± 0.3
Leakage volume [mL]	3.11 ± 0.31	7.63 ± 0.14
Closing volume [mL]	3.25 ± 0.30	2.23 ± 0.11

A_{EO} indicates effective orifice area.

Table S2. *In vivo* evaluation of progress of pulmonary valve regurgitation during 12 months follow-up of each individual animal. Pulmonary regurgitation was graded as none (0), mild (1), moderate (2) or severe (3). Bold letter indicated epicardial echocardiographic evaluation at time of implantation and explantation. Regular letter type TTE. #12.7 and #12.8 were excluded cause of endocarditis. #1.4 died due to OR complications.

Method		Epicardial echo	Trans thoracic echo **(Epicardial echo at end of follow-up)**					
Time (months)		Implantation	1	2	4	6	9	12
aTEHV	1.2	**0**	0 **(0)**	-	-	-	-	-
	1.3	**0**	0 **(0)**	-	-	-	-	-
	6.5	**0**		0	1	1 **(1)**	-	-
	6.6	**0**		1	2	1 **(1)**	-	-
	6.8	**1**		1	2	2 **(2)**	-	-
	6.7	**0**		0	0	0 **(2)**	-	-
	12.1	**0**		0	0	0	1	1 **(2)**
	12.2	**0**		1	1	1	2	2 **(2)**
	12.7	**1**	*Endocarditis*					
	12.8	**0**	*Endocarditis*					
rTEHV	1.1	**0**	1 **(1)**	-	-	-	-	-
	1.4	**1**	*Drop off +1day*					
	6.1	**0**		1	0	2 **(3)**	-	-
	6.2	**0**		0	2	2 **(3)**	-	-
	6.3	**1**		0	0	0 **(2)**	-	-
	6.4	**0**		0	0	0 **(1)**	-	-
	12.3	**0**		0	0	0	0	1 **(2)**
	12.4	**1**		0	0	0	1	1 **(2)**
	12.5	**0**		0	0	0	0	0 **(1)**
	12.6	**1**		1	0	0	1	1 **(2)**

Table S3. Individual data of invasive transvalvular systolic peak pressure assessment direct after implantation and before explantation of the TEHVs. rTEHV; random Tissue engineered heart valve. aTEHV;aligned Tissue engineered heart valve. *PG; Peak pressure gradient.*

rTEHV			**aTEHV**		
	Transvalvular PG (mmHg)			Transvalvular PG (mmHg)	
Animal	Implantation	Explantation	Animal	Implantation	Explantation
#1.1	5	25	#1.2	2	18
#1.4	3	*missing*	#1.3	13	14
#6.1	12	10	#6.5	*missing*	17
#6.2	13	7	#6.6	2	18
#6.3	3	*missing*	#6.7	7	15
#6.4	1	8	#6.8	5	23
#12.3	3	25	#12.1	*missing*	38
#12.4	*missing*	17	#12.2	1	14
#12.5	6	6	#12.7	9	*Endocarditis*
#12.6	*missing*	7	#12.8	11	*Endocarditis*

SUPPLEMENTARY FIGURES and FIGURES LEGENDS

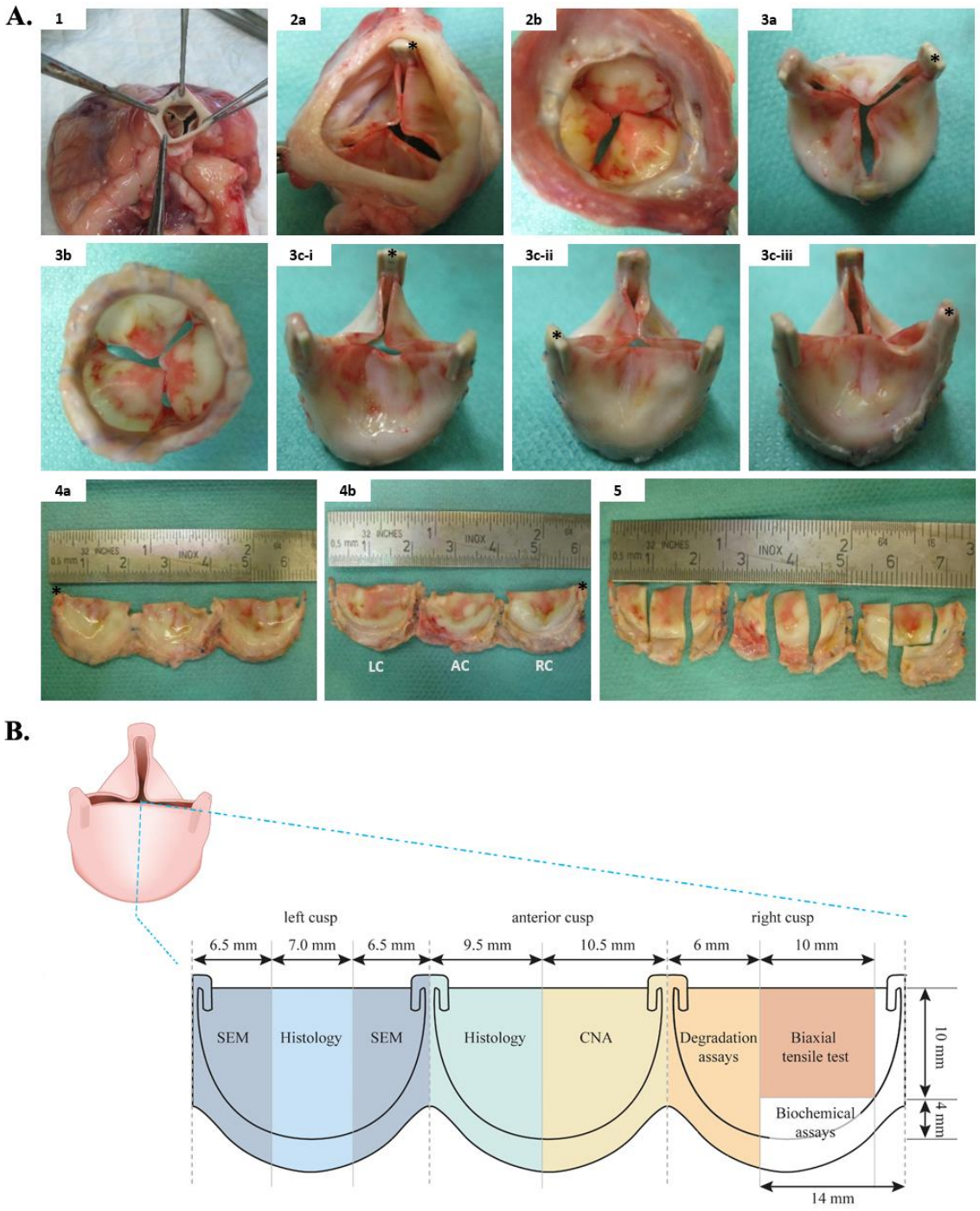

Figure S1. (A) Representative photographs of explant treatment according to standard operating procedures, with the valve *in situ* (1); the valve in the pulmonary artery explanted from the heart, pulmonary (2a) and ventricular view (2b); the valve isolated from the artery, pulmonary view (3a), ventricular view (3b), and side view on each leaflet (3c, with i representing the left cusp, ii the anterior cusp, and iii the right cusp); longitudinally opened valve after removal from the PEEK stent, pulmonary (4a) and ventricular side (4b); the valve sectioned according to the cutting scheme (5). * indicates the strut between left and right cusp for longitudinal sectioning. **(B)** Schematic example of the cutting scheme.

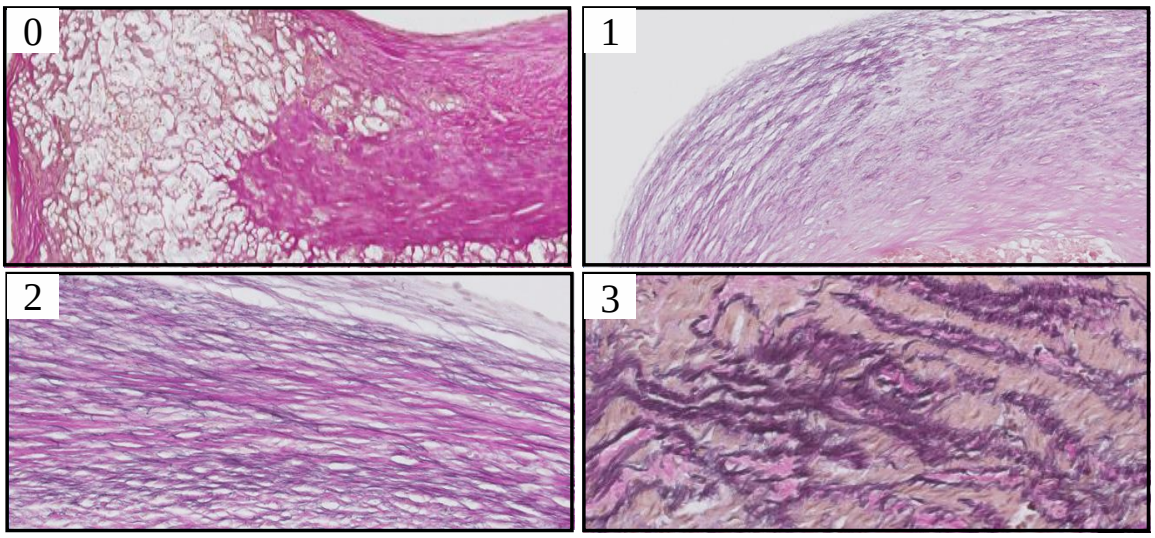

Figure S2: **Elastin classification**; None (0), thin/few fibers (1), thin/moderate fibers (2), native-like fibers (3).

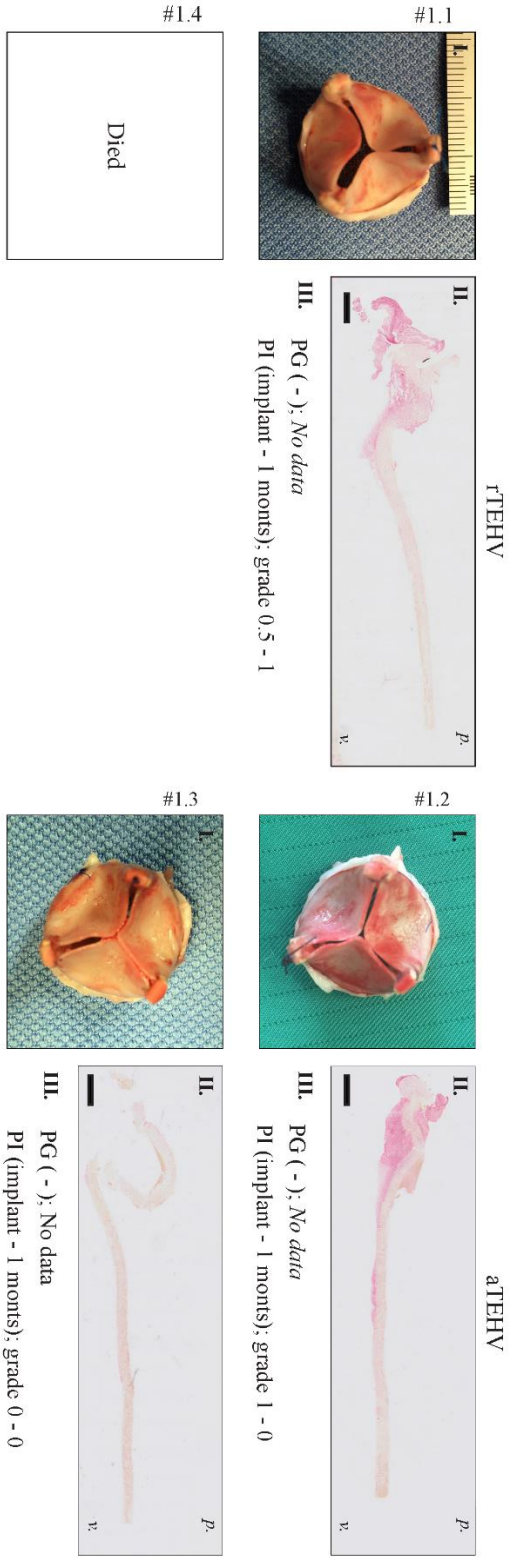

Figure S3. Macroscopic appearance **(I.)**, histological tile scan of collagen formation **(II.)** and functional results **(III.)** of individual explanted rTEHV and aTEHV valves after **one month**. The macroscopic evaluation **(I.)** showed smooth leaflets in absence of (non-)structural valve deterioration (e.g. tears or irregularities) in both groups. Tile scan of the picrosirius red staining **(II.)** shows early de novo collagen formation in particular in the lower wall and hinge regions in both groups. There were no apparent differences between the PR grade **i**n both groups **(III.)**. *PG; peak pressure gradient. PR; pulmonary regurgitation. P; pulmonary side. V; ventricular side.*

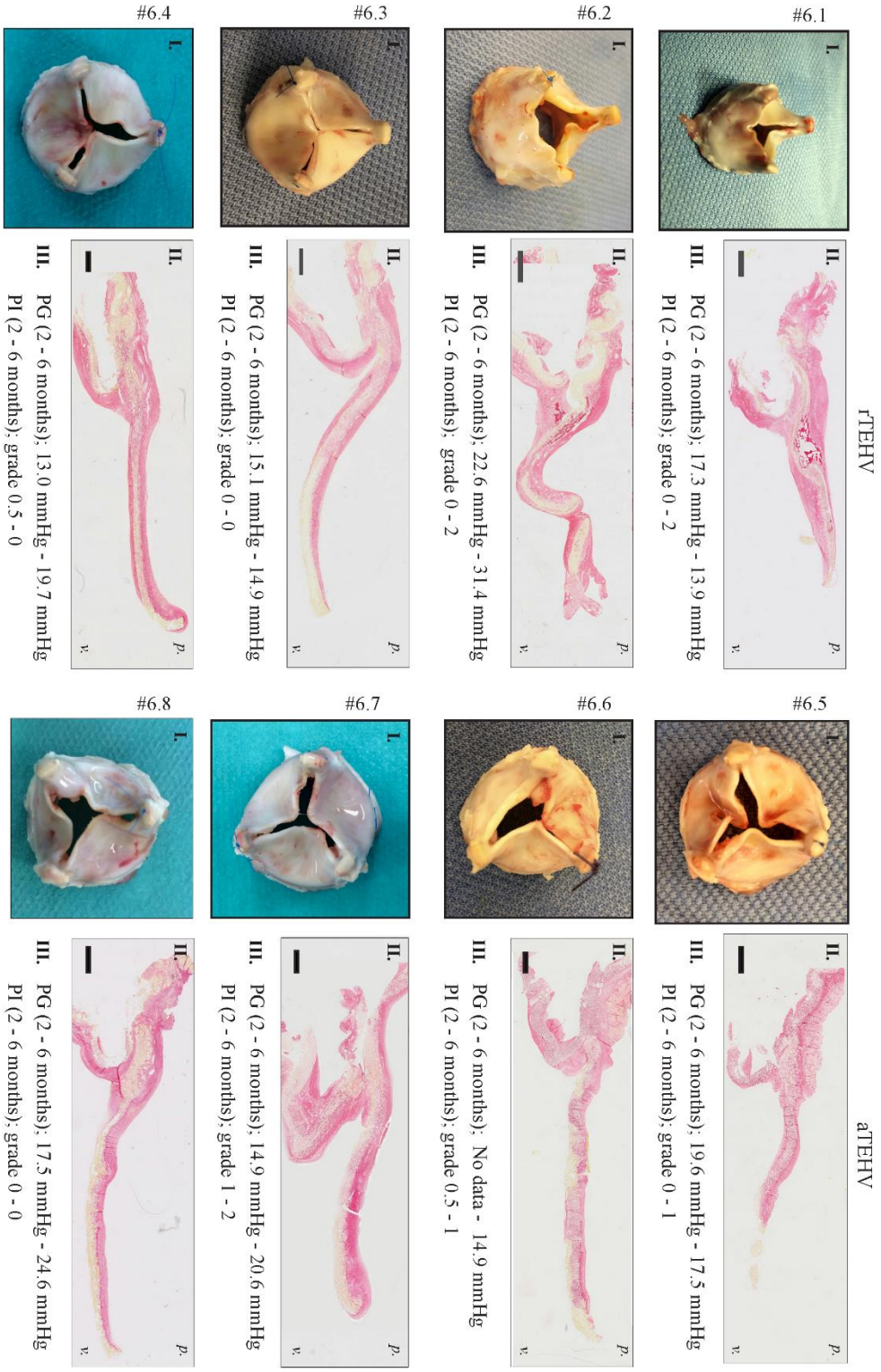

Figure S4. Macroscopic appearance **(I.),** histological tile scan of collagen formation **(II.)** and functional results **(III.)** of individual rTEHV and aTEHV valves after **six months.** The macroscopic evaluation **(I.)** showed valve-to-valve variation within and between the two scaffold groups, with cases with absence of (non-)structural valve deterioration (e.g. tears or irregularities) in contrast to valves with leaflet retraction (#6.2) or tears (#6.5). Tile scans of the picrosirius red staining **(II.)** show increase of collagen formation in both groups. Particular located at the pulmonary side *(p.)* of the leaflet that was distributed from hinge to the tip. The aTEHV showed a trend in higher PG when compared to the rTEHV at 6 months **(III.)**. There were no apparent differences between the PR grade in both groups. *PG; peak pressure gradient. PR; pulmonary regurgitation. P; pulmonary side. V; ventricular side.*

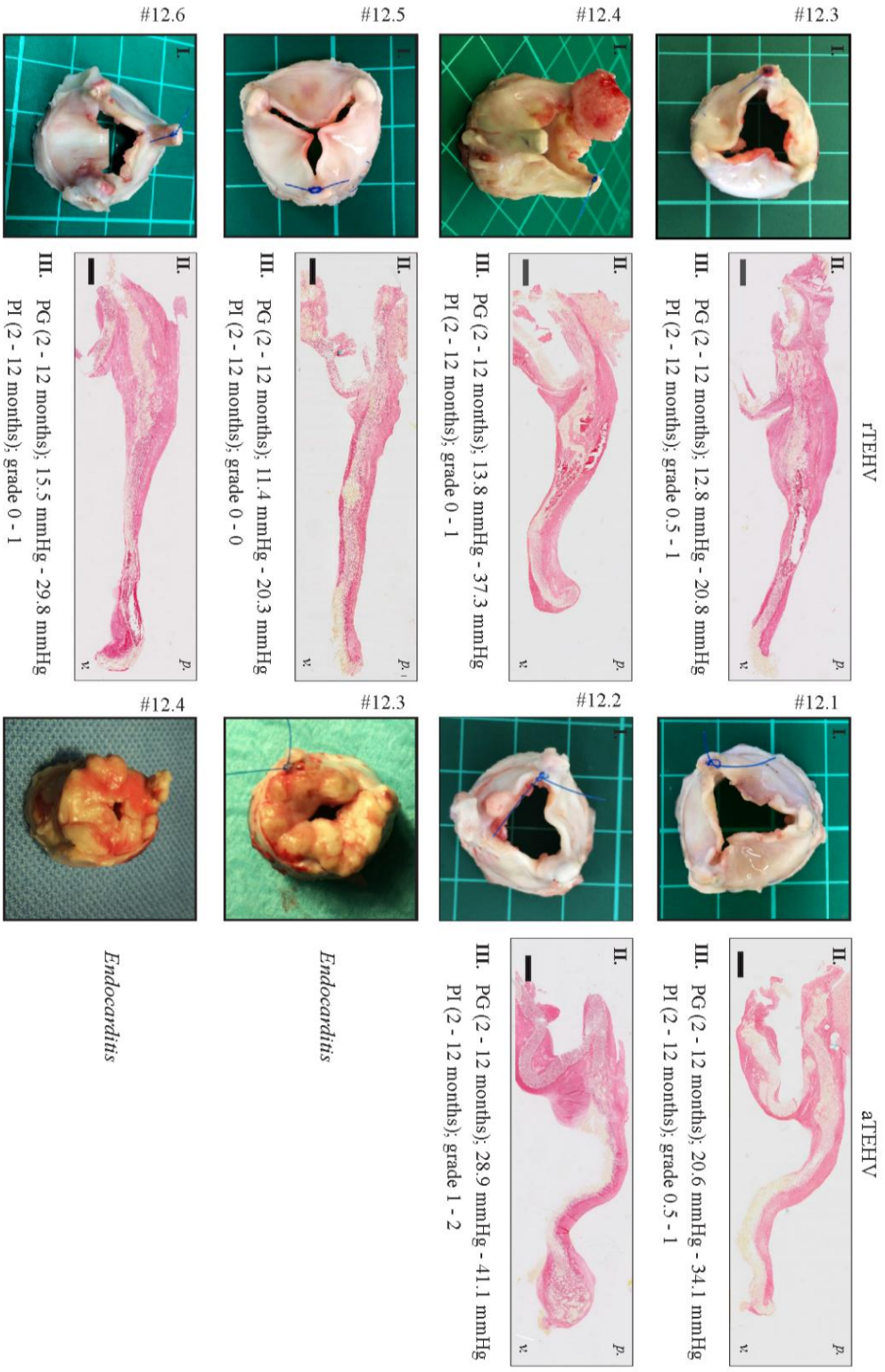

Figure S5. Macroscopic appearance **(I.),** histological tile scan of collagen formation **(II.)** and functional results **(III.)** of individual explanted rTEHV and aTEHV valves at **<u>12 months</u>**. The macroscopic evaluation **(I.)** showed valve-to-valve variation within and between the two scaffold groups, with cases with absence of (non-)structural valve deterioration (e.g. #12.5) in contrast to valves with for example noduli (#12.2 and #12.4). Tile scans of the picrosirius red staining **(II.)** show stable amount of collagen that was predominantly located at the pulmonary side of the leaflet and distributed from hinge to the tip. Both groups showed an increase of the PG gradients compared to the six months results with a consistent trend of higher gradients in the aTEHV group **(III.)**. *PG; peak pressure gradient. PR; pulmonary regurgitation. P; pulmonary side. V; ventricular side.*

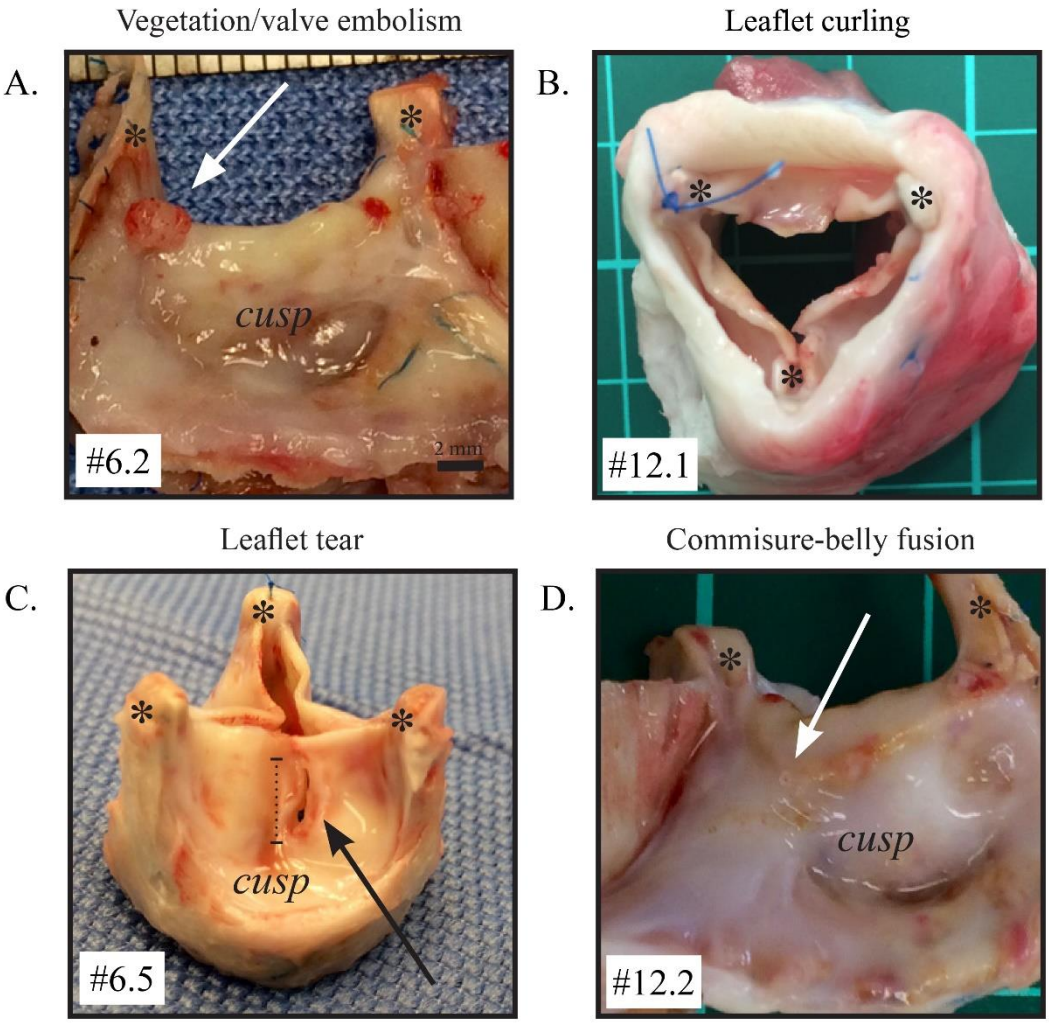

Figure S6. Representative examples of structural valve deterioration in explanted valves at 6 **(A, C)** and 12 months **(B, D).** * indicate the commissure area.

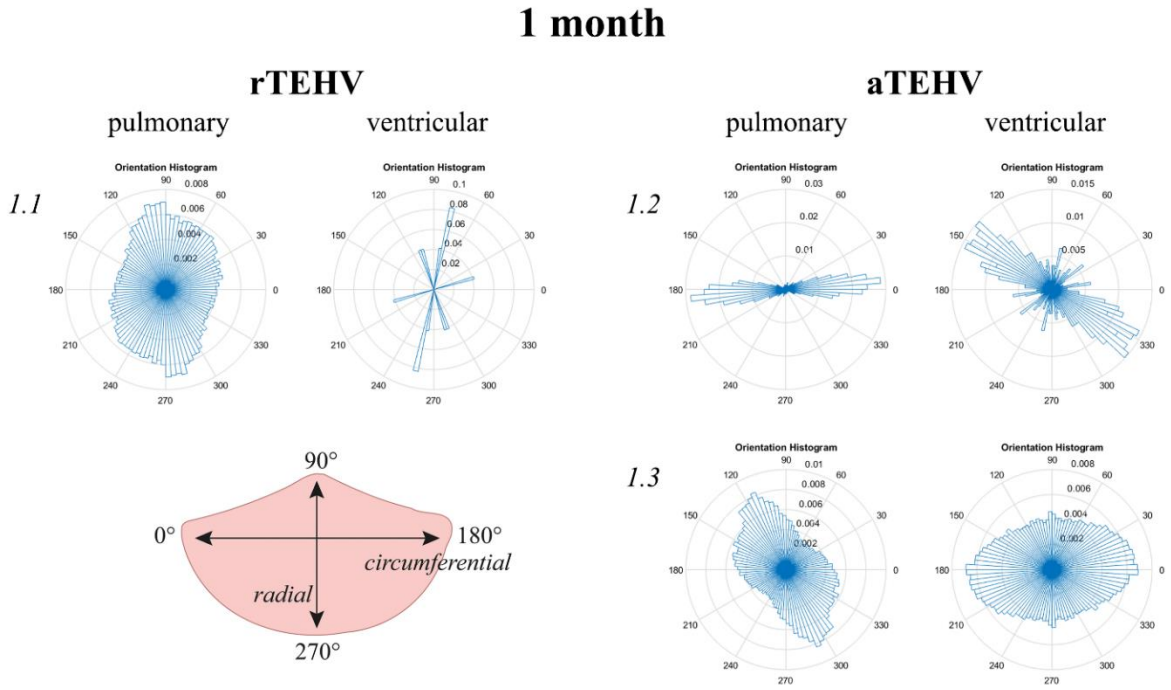

Figure S7. Orientation rosettes representing the quantification of collagen orientation in the superficial layers of the valve leaflet from *en face* visualization by confocal microscopy (CNA staining) on both the pulmonary and the ventricular side of the leaflet in the random (rTEHV) and aligned (aTEHV) tissue-engineered heart valves after 1 month of implantation. 0 and 180 degrees correspond to the circumferential direction and 90 and 270 degrees to the radial direction of the leaflet as indicated schematically (bottom right).

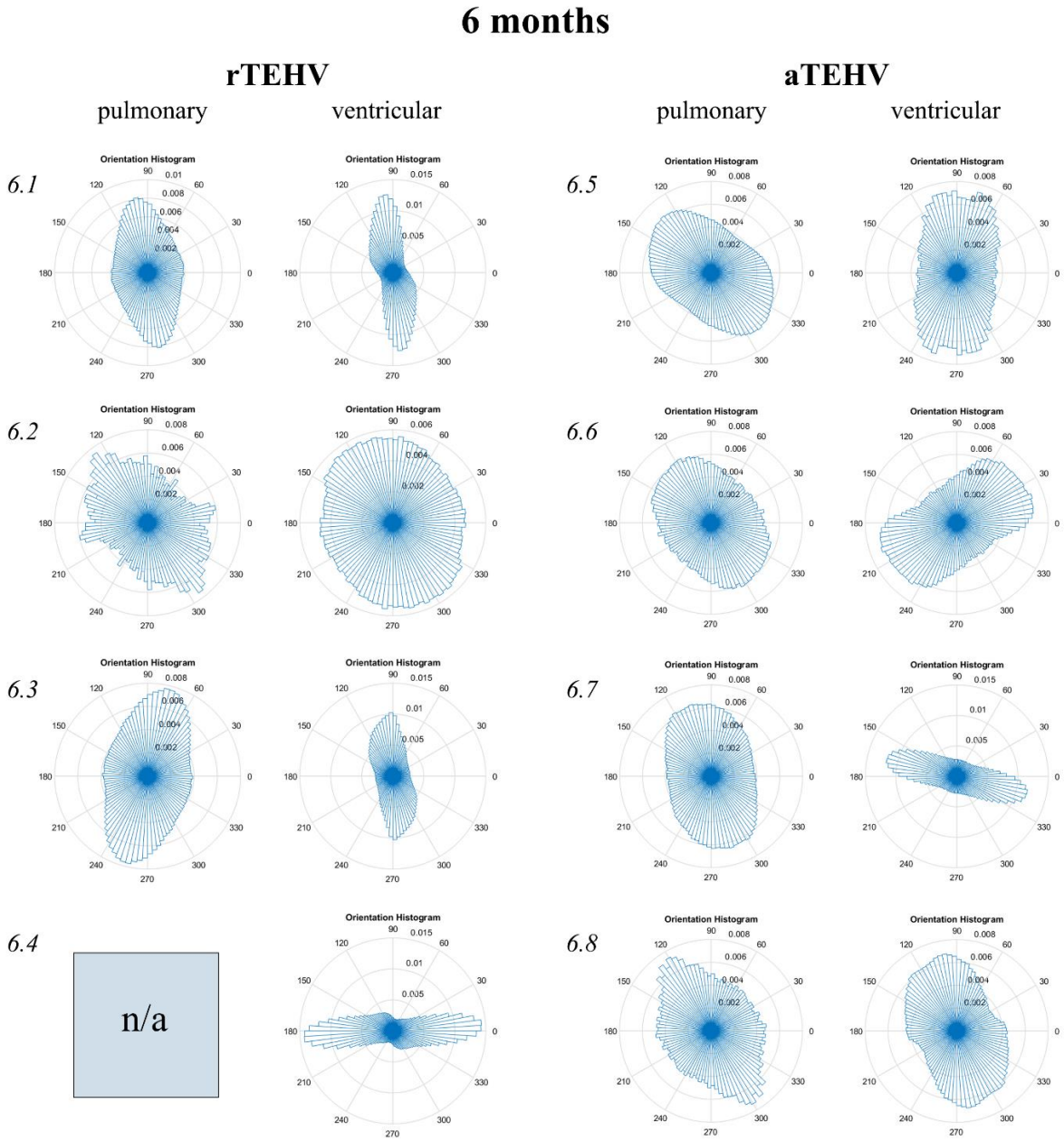

Figure S8. Orientation rosettes representing the quantification of collagen orientation in the superficial layers of the valve leaflet from *en face* visualization by confocal microscopy (CNA staining) on both the pulmonary and the ventricular side of the leaflet in the random (rTEHV) and aligned (aTEHV) tissue-engineered heart valves after 6 months of implantation. 0 and 180 degrees correspond to the circumferential direction and 90 and 270 degrees to the radial direction of the leaflet as indicated schematically (bottom right).

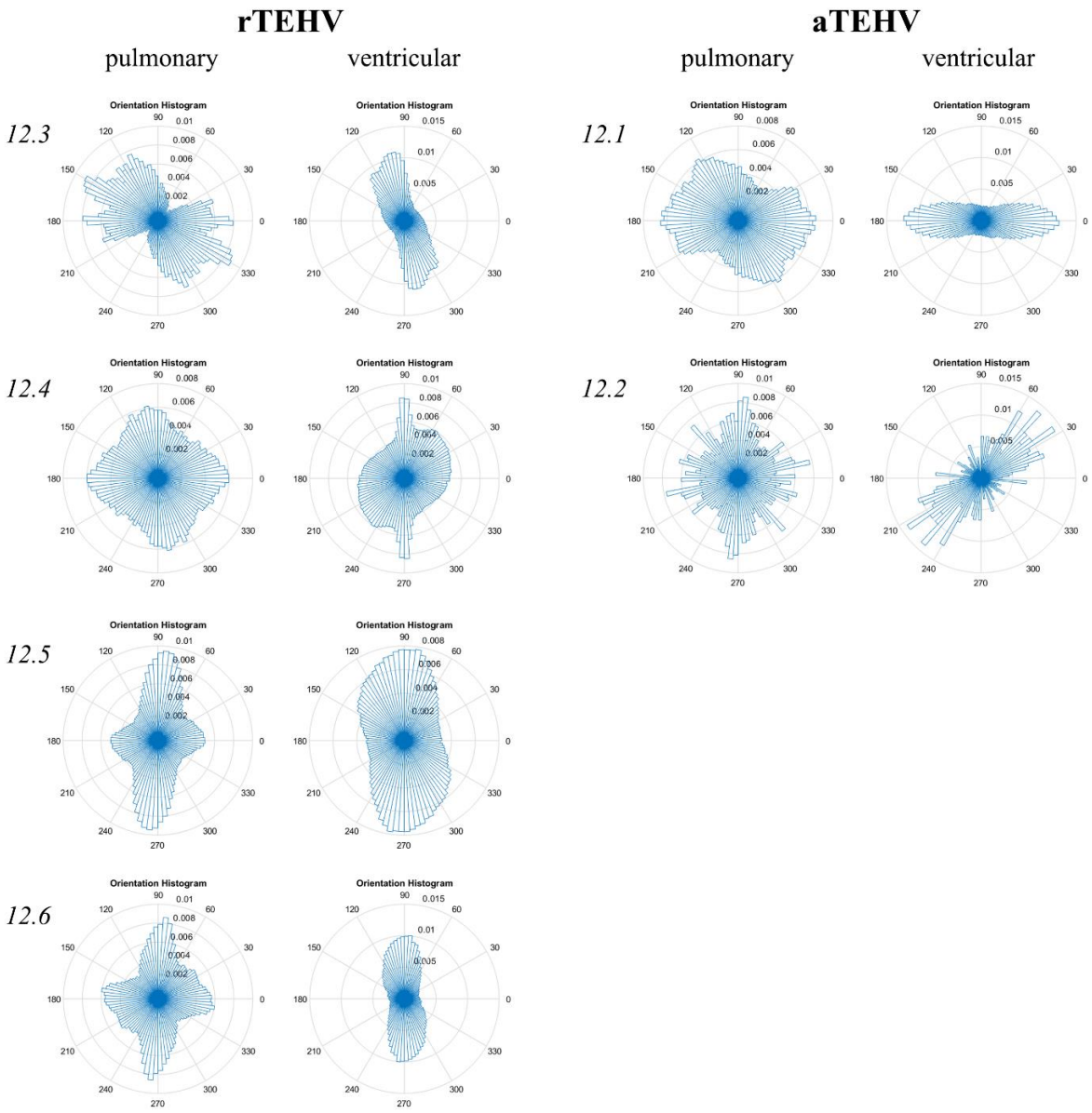

Figure S9. Orientation rosettes representing the quantification of collagen orientation in the superficial layers of the valve leaflet from *en face* visualization by confocal microscopy (CNA staining) on both the pulmonary and the ventricular side of the leaflet in the random (rTEHV) and aligned (aTEHV) tissue-engineered heart valves after 12 months of implantation. 0 and 180 degrees correspond to the circumferential direction and 90 and 270 degrees to the radial direction of the leaflet as indicated schematically (bottom right).

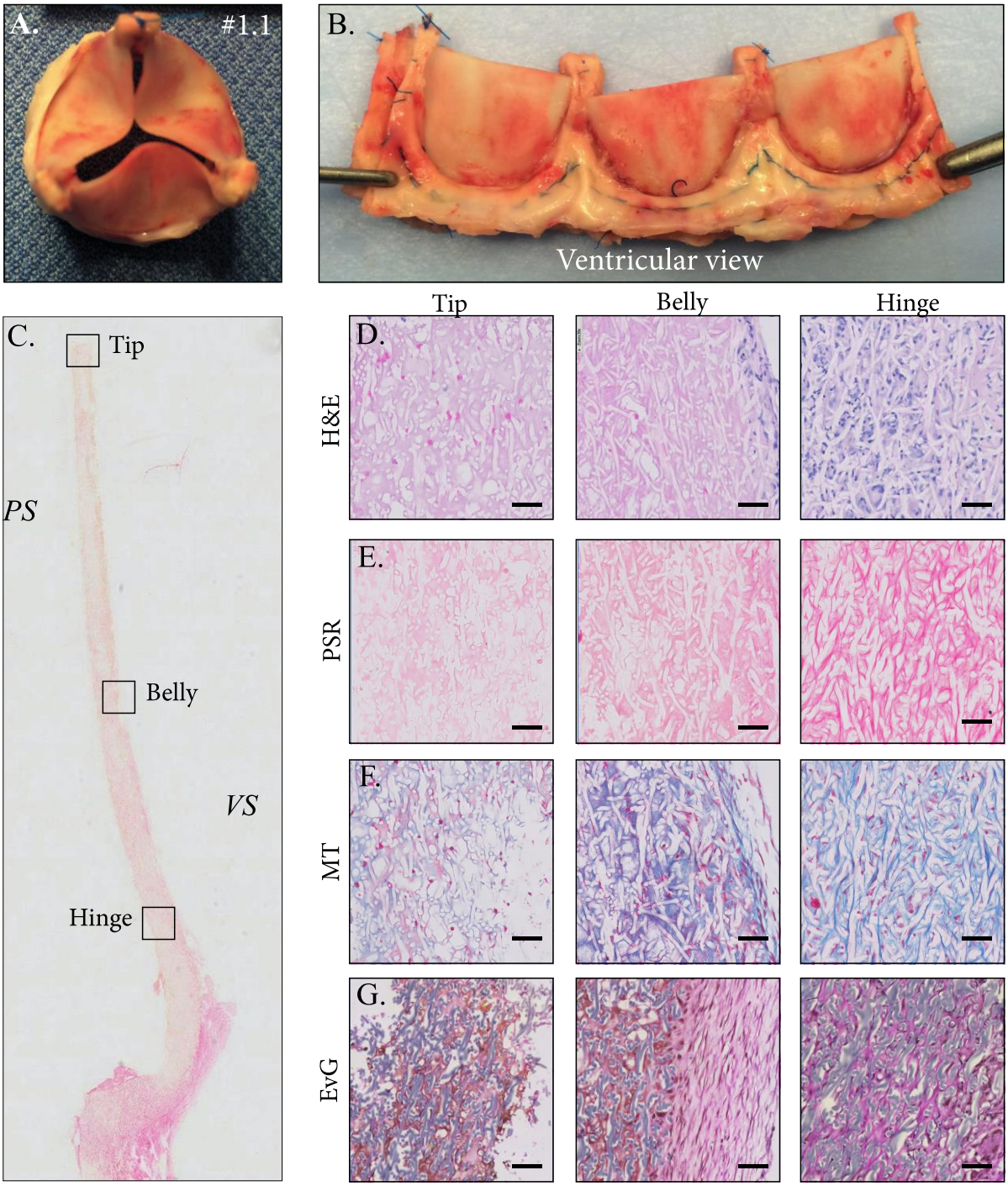

Figure S10. Histological results of a random TEHV at 1 month (#1.1). (**A**) Explant from distal view (**B**) and longitudinally opened. (**C**) Tile scan of picrosirius red staining showing collagen formation (pink) and presence of scaffold material (white-yellow). *PS*, pulmonary side; *VS*, ventricular side. (**D-G**) High power field of hinge, belly and tip region, showing limited cell infiltration at tip and belly region, and early cell infiltration in the hinge region (D; Hematoxylin & Eosin staining, H&E, with cell nuclei in blue). Extracellular matrix stainings show limited tissue formation at 1 month, progressing from the hinge to the tip (E; Picrosirius Red staining, PSR, with collagen in pink; and F, Masson's Trichrome staining, MT, with collagen in blue, cell nuclei in black, cytoplasm in pink). No formation of elastin was seen at this time point (G; Elastica van Gieson, EvG, with elastin in black). Scale bars represent 100 µm.

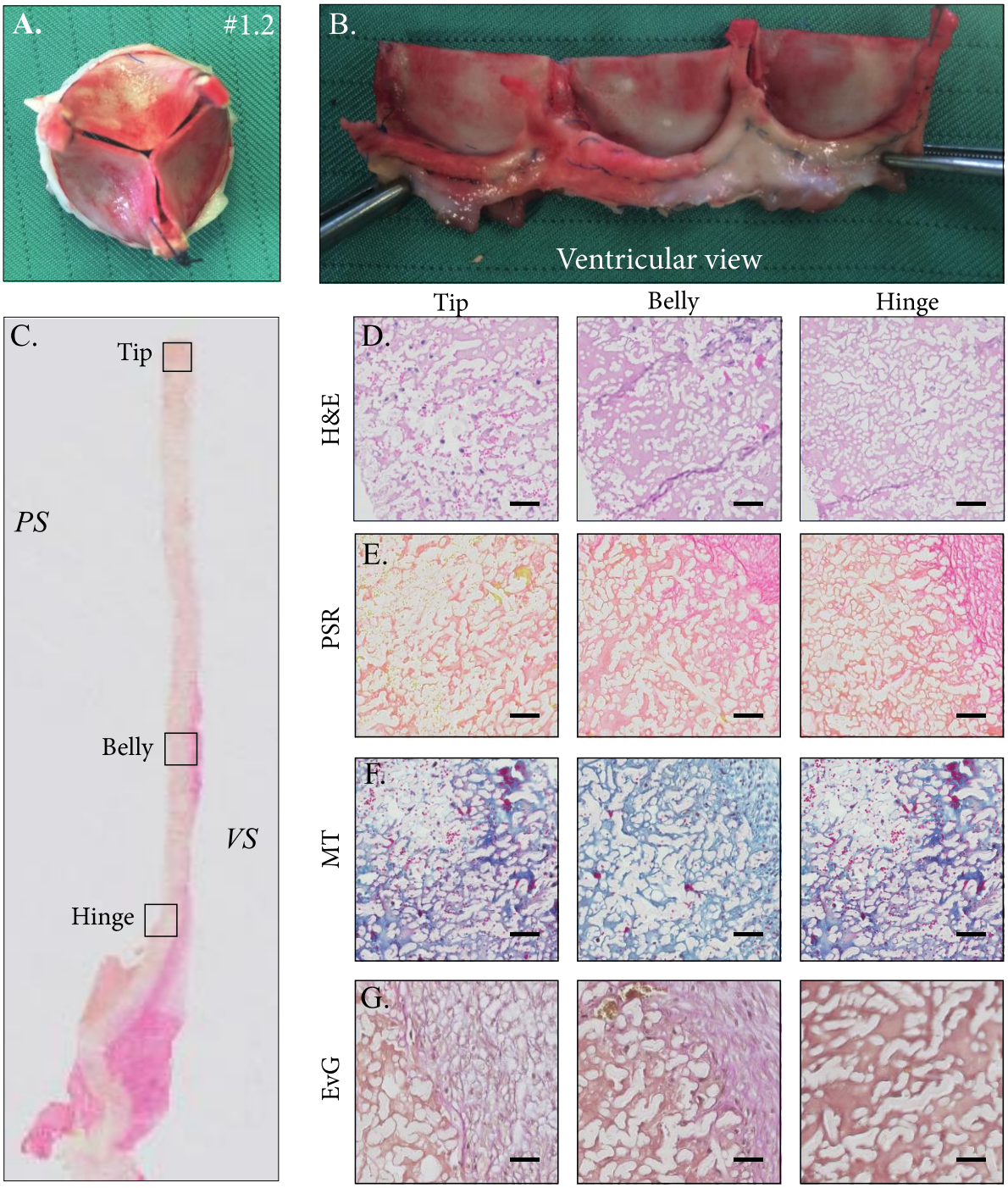

Figure S11. Histological results of an aligned TEHV at 1 month (#1.2). (**A**) Explant from distal view (**B**) and longitudinally opened. (**C**) Tile scan of picrosirius red staining showing collagen formation (pink) and presence of scaffold material (white-yellow). *PS*, pulmonary side; *VS*, ventricular side. (**D-G**) High power field of hinge, belly and tip region, showing limited cell infiltration in all regions (D; Hematoxylin & Eosin staining, H&E, with cell nuclei in blue). Extracellular matrix stainings show limited tissue formation at 1 month (E; Picrosirius Red staining, PSR, with collagen in pink; and F, Masson's Trichrome staining, MT, with collagen in blue, cell nuclei in black, cytoplasm in pink). No formation of elastin was seen at this time point (G; Elastica van Gieson, EvG, with elastin in black). Scale bars represent 100 µm.

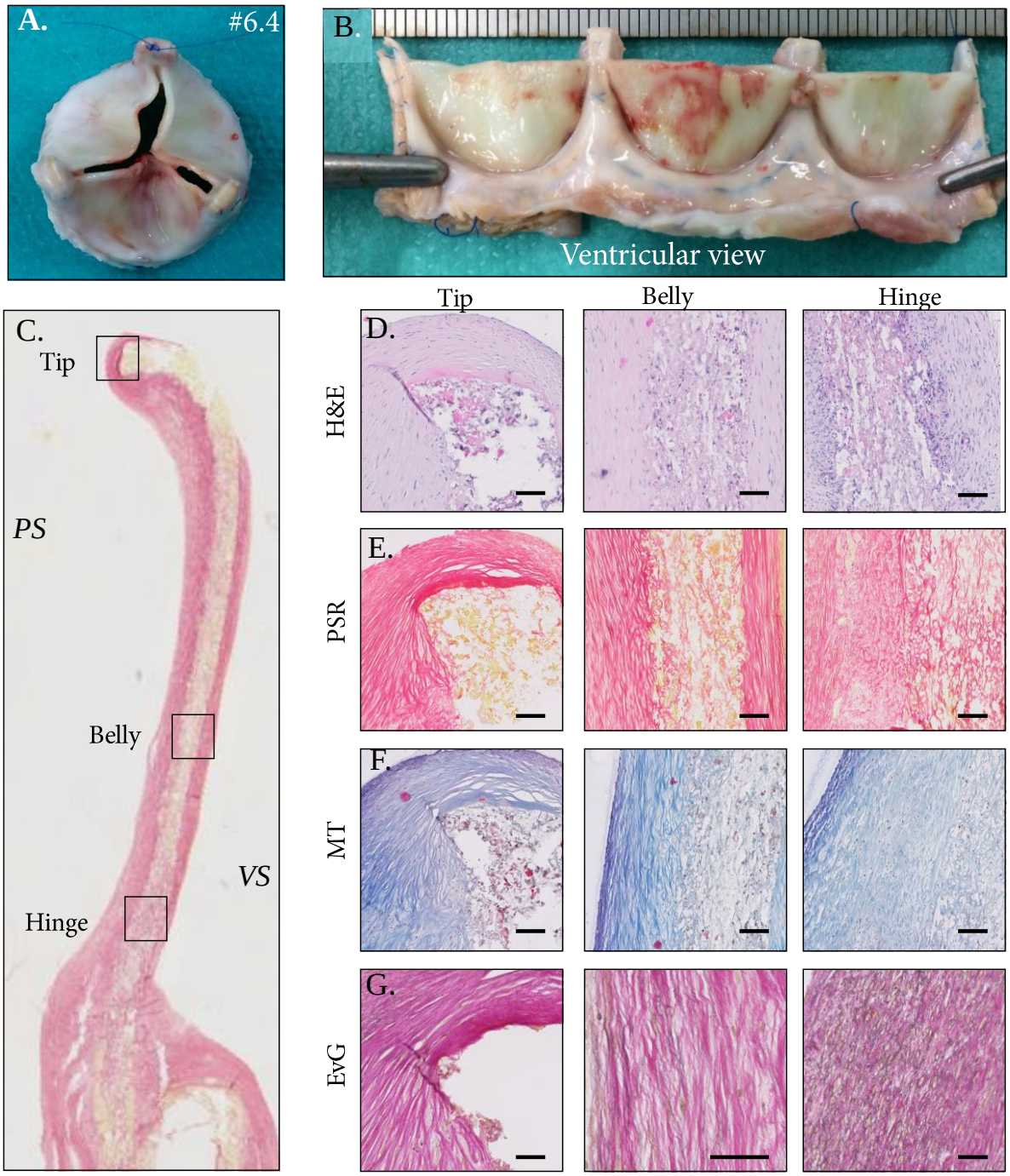

Figure S12. Histological results of a random TEHV at 6 months (#6.4). (**A**) Explant from distal view (**B**) and longitudinally opened. (**C**) Tile scan of picrosirius red staining showing collagen formation (pink) and presence of scaffold material (white-yellow). *PS*, pulmonary side; *VS*, ventricular side. (**D-G**) High power field of hinge, belly and tip region, showing extensive cell infiltration in all regions (D; Hematoxylin & Eosin staining, H&E, with cell nuclei in blue). Extracellular matrix stainings show extensive tissue formation in between scaffold fibers, as well as pannus overgrowth on both sides of the leaflet (E; Picrosirius Red staining, PSR, with collagen in pink; and F, Masson's Trichrome staining, MT, with collagen in blue, cell nuclei in black, cytoplasm in pink). Few thin elastin fibers were detected at the hinge and belly regions (G; Elastica van Gieson, EvG, with elastin in black). Scale bars represent 100 µm.

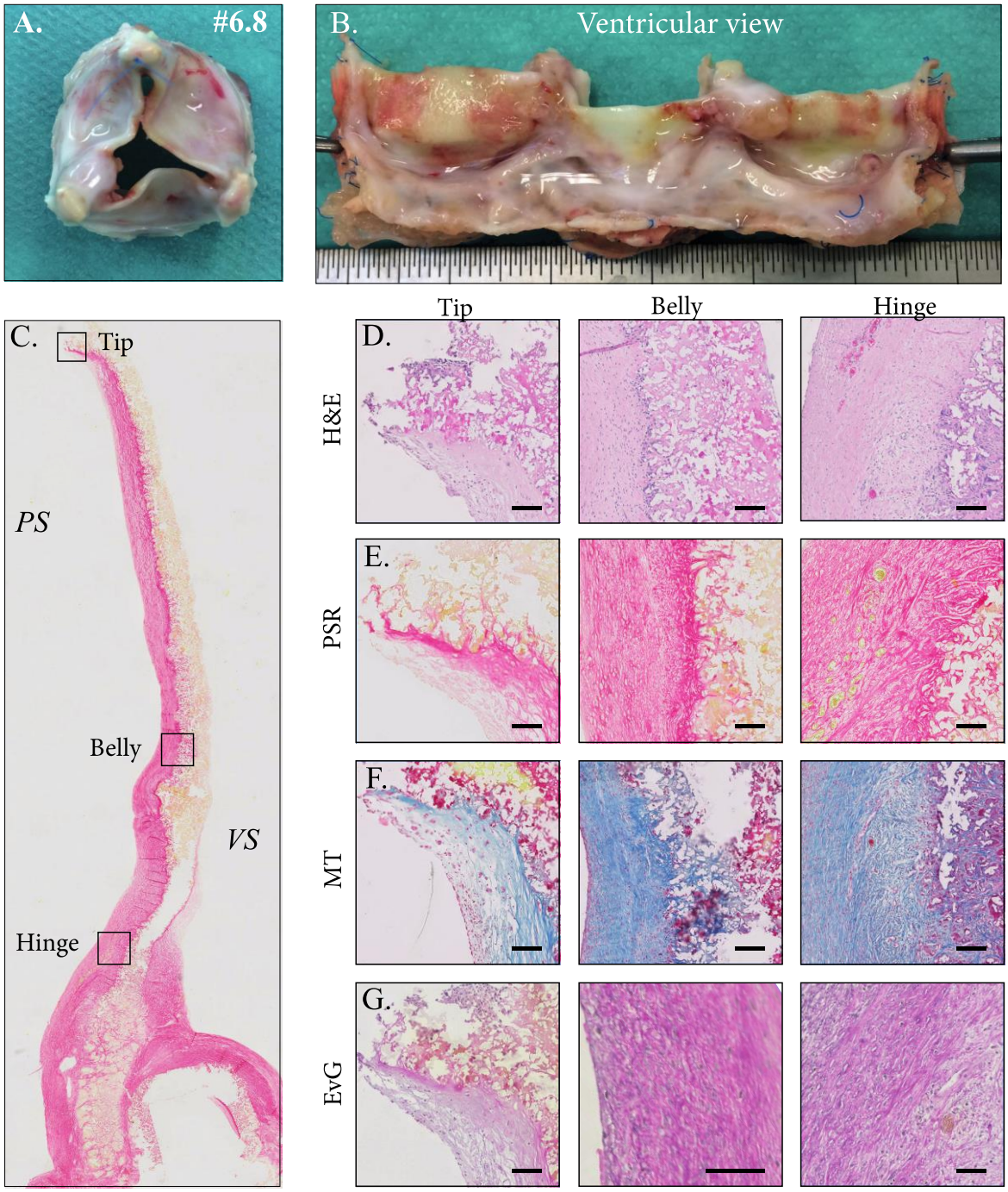

Figure S13. Histological results of an aligned TEHV at 6 months (#6.8). (**A**) Explant from distal view (**B**) and longitudinally opened. (**C**) Tile scan of picrosirius red staining showing collagen formation (pink) and presence of scaffold material (white-yellow). *PS*, pulmonary side; *VS*, ventricular side. (**D-G**) High power field of hinge, belly and tip region, showing extensive cell infiltration in all regions (D; Hematoxylin & Eosin staining, H&E, with cell nuclei in blue). Extracellular matrix stainings show pannus overgrowth, predominantly on the pulmonary side of the leaflet, with limited collagen deposition within the scaffold (E; Picrosirius Red staining, PSR, with collagen in pink; and F, Masson's Trichrome staining, MT, with collagen in blue, cell nuclei in black, cytoplasm in pink). No elastin fibers were detected in this valve (G; Elastica van Gieson, EvG, with elastin in black). Scale bars represent 100 µm.

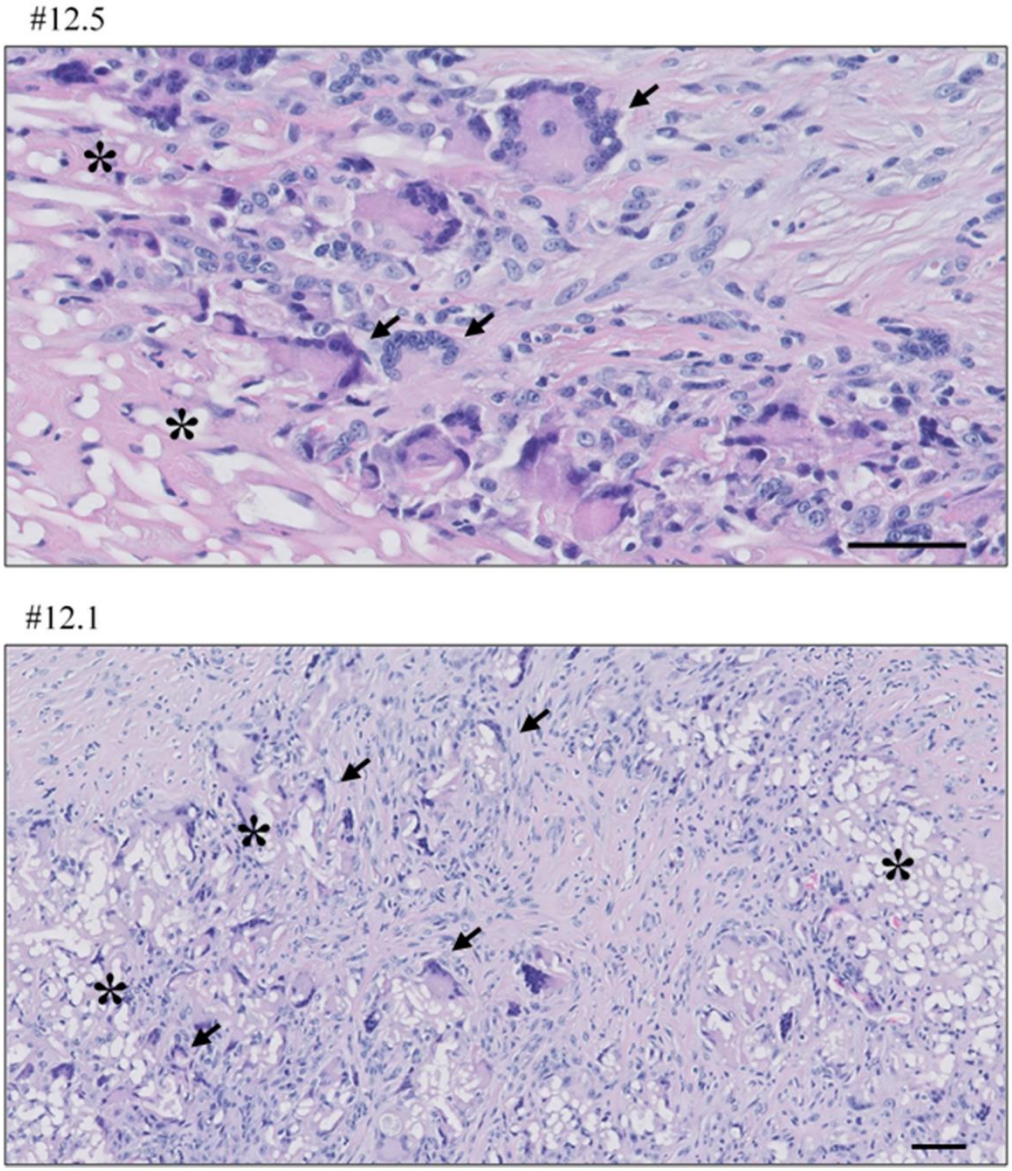

Figure S14. Examples of multinucleated giant cell formation. Representative image of giant cells in a rTEHV (#12.5) and aTEHV (# 12.1) in H&E staining. Fusion of immune cells (black arrow) are located at the border of scaffold fibers remnants (*) and neo-tissue formation. Scale bars 50µm.

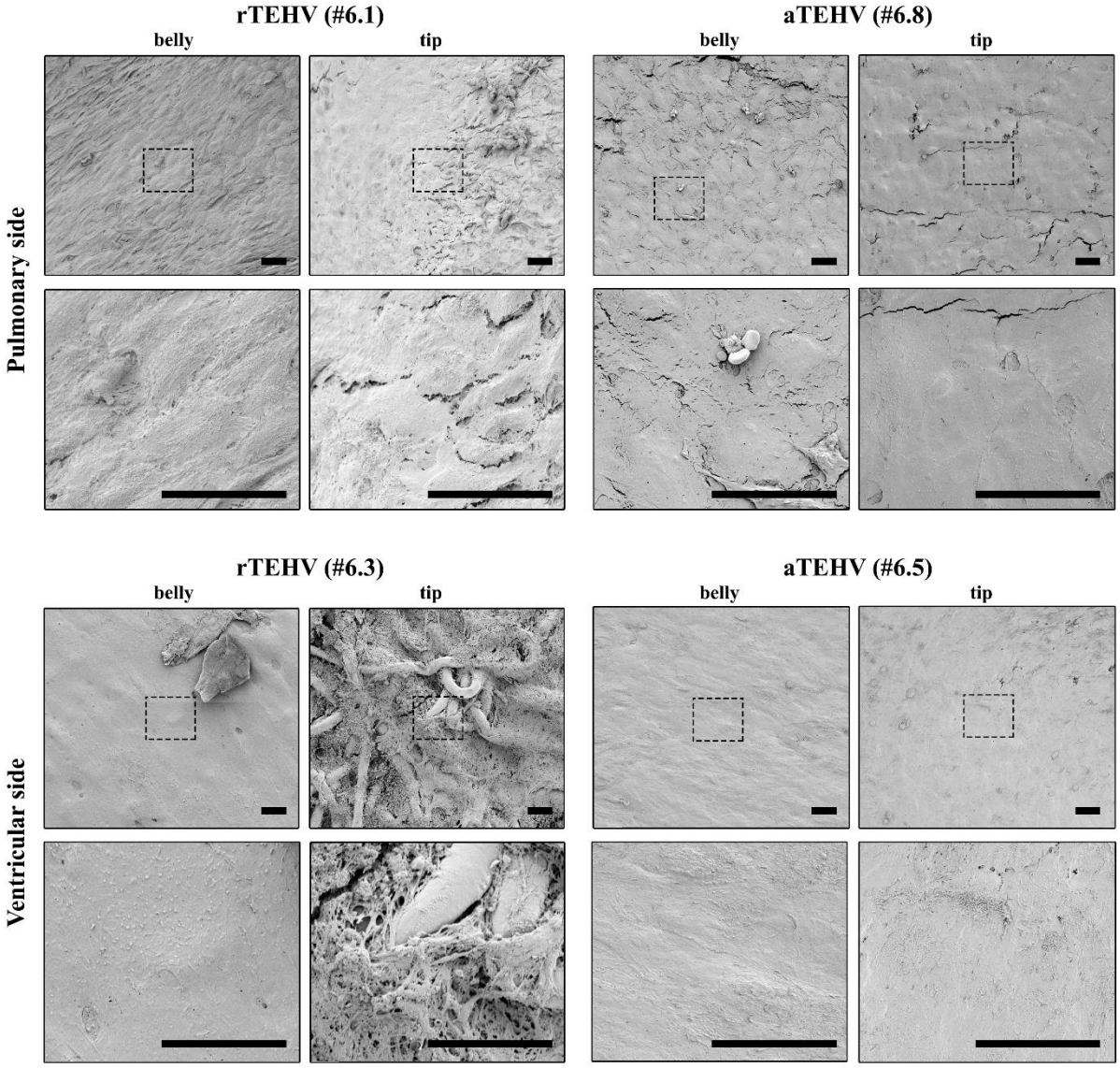

Figure S15. Representative SEM imags in the belly and tip regions of the pulmonary (top panel) and ventricular (bottom panel) side of the valve leaflets of rTEHVs (left column) and aTEHVs (right column) after 6 months *in vivo*. Scaffold coverage by an endothelial monolayer is evident in most regions, whereas exposed scaffold fibers are visible in localized regions of most valves, particularly near the leaflet tip (e.g. #6.3, ventricular side). Scale bars represent 25 µm.

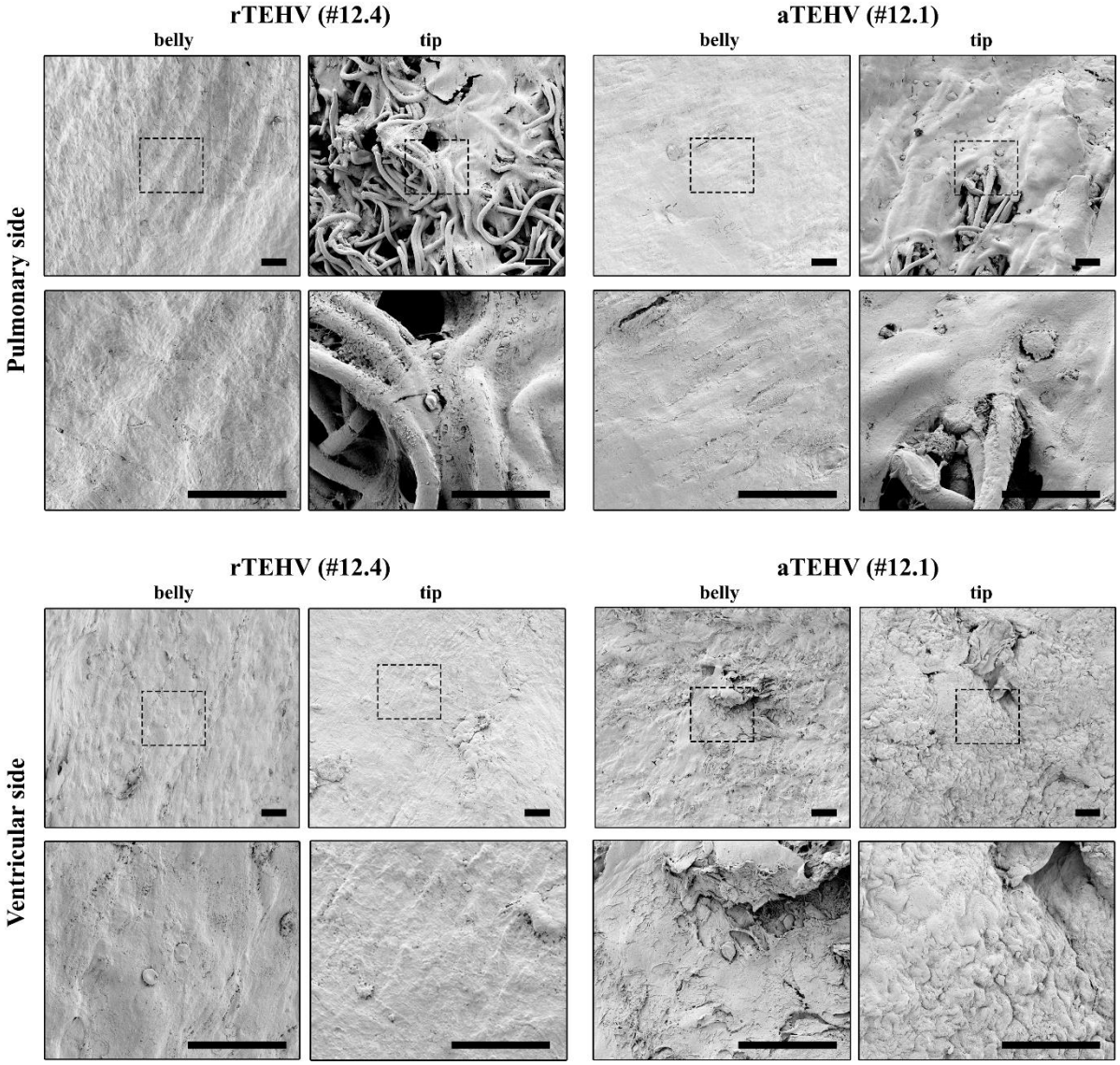

Figure S16. Representative SEM images in the belly and tip regions of the pulmonary (top panel) and ventricular (bottom panel) side of valve leaflets of rTEHVs (left column) and aTEHVs (right column) after 12 months *in vivo*. Scaffold coverage by an endothelial monolayer is evident in most regions, whereas exposed scaffold fibers are visible in localized regions of most valves, particularly near the leaflet tip (e.g. #12.4 and #12.1, both pulmonary side). Scale bars represent 25 µm.

SUPPLEMENTARY VIDEOS

Supplementary Video S1. *In vitro* functionality of rTEHV in pulse duplicator (21 mm ∅ holder).

Supplementary Video S2. *In vitro* functionality of aTEHV in pulse duplicator (21 mm ∅ holder).